Chang, Bo; Feng, Yu H.; Jin, Jia L.; Zhou, Quan

Ejected Droplet-Directed Transportation and Self-Alignment of Microfibers to Micro Trenches

Published in:
Journal of Microelectromechanical Systems

DOI:
10.1109/JMEMS.2021.3099374

Published: 01/10/2021

Document Version
Peer-reviewed accepted author manuscript, also known as Final accepted manuscript or Post-print

Please cite the original version:
Chang, B., Feng, Y. H., Jin, J. L., & Zhou, Q. (2021). Ejected Droplet-Directed Transportation and Self-Alignment of Microfibers to Micro Trenches. *Journal of Microelectromechanical Systems*, *30*(5), 751-758. https://doi.org/10.1109/JMEMS.2021.3099374

Ejected Droplet-Directed Transportation and Self-alignment of Microfibers to Micro Trenches

Bo Chang, Yu H. Feng, Jia L. Jin and Quan Zhou, *Member, IEEE*

***Abstract*—Microfibers are important components in the fabrication of fiber-reinforced materials, and the distribution and alignment of microfibers can affect the mechanical, electrical, and thermal properties of the fiber-reinforced materials. However, it remains a challenge to precisely align and distribute microfibers on a large scale at a high throughput. This paper reports a facile droplet-directed method to transport and self-align microfibers to micro trenches using droplets ejected from a non-contact dispenser. Employing super hydrophilic-super hydrophobic trenches with sizes matching the microfibers, the method can align and transport randomly dispersed fibers around trenches into the trenches as desired. We studied this alignment and transport mechanism and the results suggest that liquid volume is critical to allow the capillary force to be dominant leading to the success of the process. We demonstrated that microfibers having an aspect ratio of 200, a diameter of 15 µm and a length of 3 mm, can reliably self-align to super hydrophilic-super hydrophobic trenches and transport to the target location, achieving linear alignment accuracy of 0.5 µm and angular accuracy of 0.1°. The high accuracy and fast process of the proposed technique may greatly impact larger scale and high throughput construction of complex microstructures using microfibers.**

***Index Terms*— capillary self-alignment, microassembly, micro manipulation, microfibers, super hydrophilic-super hydrophobic patterned surfaces.**

I. Introduction

MICROFIBERS are key components in the fabrication of fiber-reinforced materials, and their distribution and alignment can affect the mechanical, [1] electrical, [2] and thermal properties [3] of fiber-reinforced materials. Many alignment methods have been reported, e.g., electrospinning [4], [5], 3D printing [6], [7], robotic manipulation [8], and microfluidics [9]. Despite of the abundance of available methods, precisely controlling the spacing and orientation of microfibers remains a challenge hampering the construction of complex patterns from microfibers.

Capillary self-alignment is a highly accurate and effecient assembly technique for microscale components. It has been demonstrated in massively parallel microassembly of semiconductor chips [10], [11] achieving sub-micron precision at great throughput and high yield [12]. Capillary self-alignment has also been used for integrating 3D microstructures, [12]–[15] GaAs blocks [16] and optoelectronic devices [17]. A comprehensive review of capillary self-alignment can be found at [18]. Noticeably, the components used in capillary self-alignment are usually chips or similar, where the aspect ratio between length and width of the object is normally far less than ten. It remains largely a question if and how capillary self-alignment can align an object having a great aspect ratio between length and width.

Recently, we have shown that microfibers can be aligned to microgrooves aided by a capillary gripper [19], [20]. The results of this initial investigation are promising. However, the nature of capillary gripping involves pick-and-place of individual microfibers, which is highly versatile, but the manipulation requires careful control, and the placement of the fibers needs to be accurate, both are hampering the throughput of the process.

This work suggests a facile droplet-directed method to transport and self-align microfibers to micro trenches using droplets ejected from a non-contact dispenser. Employing super hydrophobic substrate with super hydrophilic trenches with sizes matching the microfibers, the methods can align and transport randomly dispersed fibers around trenches into the trenches as desired. The proposed method requires no precise control over initial location of the fiber, neither the actual location of the point of cross of the fiber on the trench, but only the fiber being partially on the trench and the liquid being ejected into the trench. The aspect ratio of 200 between length and width of the microfiber also brings interesting question on the mechnism of the capillary self-alignment and transportation process, compared to the previous well-studied process focused mostly on structures with a small aspect ratio of much less than ten.

The schematic of the proposed droplet-directed self-

This research was supported by the National Natural Science Foundation of China (grant no. 61703255).

Bo Chang, Yu H. Feng and Jia L. Jin are with the School of Mechanical and Electrical Engineering, Shaanxi University of Science and Technology, Xi'an, 710021 CHINA (e-mail: 1905003@sust.edu.cn; 1905004@sust.edu.cn; changbo@sust.edu.cn).

Quan Zhou is with the School of Electrical Engineering, Aalto, AALTO 00076, FINLAND (e-mail: quan.zhou@aalto.fi) .

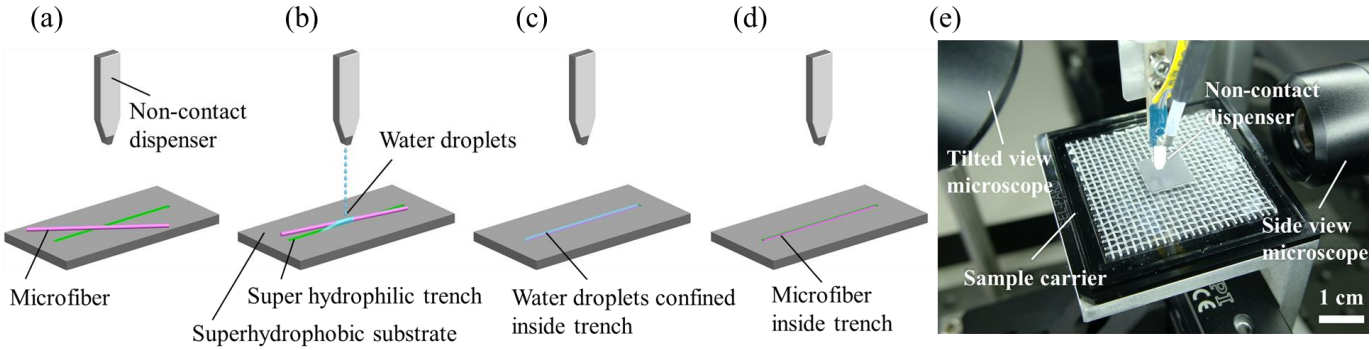

Fig. 1. Schematic and system setup of droplet directed transportation and self-alignment of microfiber: (a) a microfiber is randomly placed next to a super hydrophilic-super hydrophobic trench; (b) a non-contact dispenser ejects a series of water droplets in the trench forming a meniscus and the water meniscus quickly spreads inside the super hydrophilic trench; (c) the fiber is aligned to the fully wetted trench; (d) the fiber is transported inside the trench and the droplets evaporate; (e) robotic system for droplet directed transportation and self-alignment of microfibers on hydrophilic-super hydrophobic trench.

alignment and transportation method using a non-contact dispenser is illustrated in Fig. 1. Firstly, a microfiber is randomly placed next to a trench with the background being superhydrophobic (Fig. 1 (a)); the non-contact dispenser ejects a series of small water droplets to the trench creating a water meniscus between the microfiber and the trench, the water meniscus instantly spreads inside the super hydrophilic trench (Fig. 1 (b)); the fiber is driven by the capillary force and self-aligned to the wetted trench (Fig. 1 (c)); finally, the fiber is transported inside the trench and the water droplets evaporate (Fig. 1 (d)).

II. Experimental Setup and Test Samples

A. Experimental Setup

A robotic manipulation system has been employed to carry out the study. The system is composed of three motorized stages, a non-contact droplet dispenser and two microscopes, as shown in Fig. 1 (e). Three motorized stages (two M-111.1DG and one M-414.2PD by Physik Instrumente) were used in the system, moving the sample carrier in x-, y- and z- axis. The non-contact (Gesim/PicPIP) actuated by a piezoelectric diaphragm can eject droplets to the samples in a distance of a few millimeters. The experiments were imaged from a side view microscope (Edmund/VZM1000i) and a tilted view microscope (Edmund/VZM600i). Two CCD video cameras (Point Grey GS3-U3-23S6M-C, BFLY-U3-23S6C-C) were attached to the side view microscope and the tilted view microscope.

B. Test Samples

Glass fibers having a diameter of 15 ± 1 µm and a length of about 3 mm were used for the alignment tests. The water contact angle of the glass fiber is 50°. The super hydrophilic trenches were fabricated on super hydrophobic silicon substrates using laser micro-machining. The super hydrophobic substrate was prepared by spraying a commercial superhydrophobic coating (WHOLE-NANO, SPN-62) on a silicon substrate followed by 24 hours drying at room temperature. The substrate was then patterned using a UV laser marking machine (HGTECH LU-5, Huagong Ltd., Wuhan, China) with 355 nm wavelength at a power of 5 W. The laser marking machine was operated with pulse width of 1 µs, current of 1 A, scanning speed of 1500 – 2000 mm/s, and frequency of 100 kHz. The fabricated trenches are 20 µm in width and 8 µm in depth. In addition, we fabricated the trenches with different water contact angle of 10°, 25°, 90°, 130° by adjusting the scanning speed from 100 mm/s to 1500 mm/s, 4000 mm/s, and 7000 mm/s respectively. Although the contact angle of an intrinsic silicon surface is about 40°, the contact angle can be altered by surface roughness making the surface super hydrophilic [21]. Firstly, the laser was set to be out of focus, so that the energy of the laser beam is greatly reduced compared to the energy from a focused laser beam. The scanning speed was then adjusted to change the morphology of the surfaces. When the scanning speed was set to 100 mm/s, the entire superhydrophobic coating and part of the silicon layer were removed, leading to trench structures that is super hydrophilic. As the scanning speed increases, the number of pulses per length decreases, and the superhydrophobic coating was removed only partially on the scanned area, leading to different wetting properties. Fig. 2 (a) - (c) show the 2D image, 3D reconstruction and the profile of the fabricated trench. It

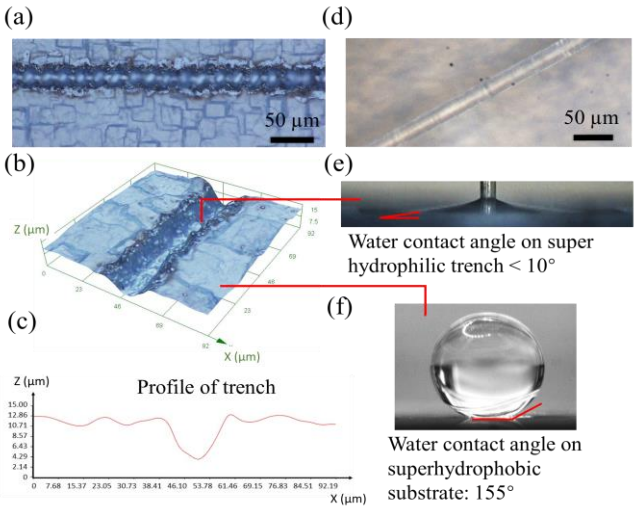

Fig. 2. Images of fabricated super hydrophilic-super hydrophobic trench and water contact angles. (a) 2D image of fabricated trench with width of 20 µm and depth of 8 µm; (b) 3D construction of fabricated trench; (c) profile of trench; (d) 2D image of glass fiber; (e) water contact angle on super hydrophilic trench; (f) water contact angle on super hydrophobic substrate.

can be clearly seen from the 3D image and the profile that the edges of the trench are jagged where the edge jaggedness has a width of about 3 μm (Fig. 2 (b)) and a height of about 2 μm (Fig. 2 (c)). The jaggedness is mainly caused by the heating effect of the UV laser marking process. The optical image of a glass microfiber is shown in Fig. 2 (d). The measured water contact angle of a super hydrophilic trench (10°) and a super hydrophobic substrate (155°) is shown in Fig. 2 (e) and (f) respectively.

III. Simulation and Analysis

The transportation and self-alignment of a microfiber to a super hydrophilic trench on a super hydrophobic substrate is driven by the capillary force of the liquid meniscus between the microfiber and the trench. The fundamental principle behind capillary self-alignment is the minimization of the surface energy. Nevertheless, the gradient of the surface energy driving the microfiber to align and transport shows interesting behaviors related to volume. Fig. 3 shows the simulations of three scenarios of a fiber lying on a trench filled with water. We used Surface Evolver [22] to simulate the liquid meniscus between a fiber and a trench by evolving the surface of the liquid meniscus using the gradient descent method. In the simulation, the diameter of the fiber is 15 μm and the width of the trench is 20 μm. The liquid media is water, with a surface tension of 72.8 mN/m.

Fig. 3 shows how the liquid volume in the trench affects the process. In the first scenario (Fig. 3 (a1)-(a3)), the water surface in the trench is below the fiber, not in contact. Therefore, no meniscus is formed between the fiber and the trench and there is no capillary force acting on the fiber. In the second scenario (Fig. 3 (b1)-(b3)), the volume of the water in the trench increases to the point where the water surface contacts the fiber and wets the fiber from the bottom and to the two sides of the fiber forming a concave meniscus, inducing force to the fiber and the consequent possible motion. To analyze the motion, we define linear placement error Δy as the position difference between the center of the microfiber and the center of the trench along the length of the trench; and rotational placement error φ as the angular difference between the fiber and the trench; and cross point of the fiber and the trench as O. Fig. 3 (b2) shows the shape of the concave meniscus between the fiber and the trench from the Surface Evolver simulation. The shape of the meniscus is determined by the actual trench shape, the volume of water, the contact angle of the fiber, the orientation of the fiber, and the gap in the vertical direction between the fiber and the trench. The capillary force that the meniscus applies to the fiber is represented by $\overrightarrow{F_C}$ which can be expressed by

$$\overrightarrow{F_C}(\Delta x, \Delta y, \Delta z) = -\nabla E(\Delta x, \Delta y, \Delta z) \quad (1)$$

where E is the surface energy of the meniscus between the fiber and the trench, and x, y, z is the displacement of the fiber along the x, y, z axes. For a given volume, the shape and size of the meniscus do not depend on the location of the cross point of the fiber and trench when the distance between the fiber and trench is fixed. Therefore, the total system energy E is translation invariant, i.e., $\nabla E(\Delta x, \Delta y) = 0$. Consequently, the net capillary force in the x- y plane on the fiber is zero, and the fiber experiences only a horizontal torque from the meniscus. The horizontal torque T_C in the x- y plane can be calculated by

$$T_c = -\mathrm{d}E/\mathrm{d}\varphi \quad (2)$$

where φ is the rotational angle of the fiber around the z-axis.

In the second scenario (Fig. 3 (b1)-(b3)), the vertical component of the capillary force acting on the fiber F_N is pointing downwards, pulling the fiber against the top surface of the trench. Consequently, the fiber experiences friction forces $f = \mu F_N$ from the trench countering the horizontal torque T_C, where μ is the friction coefficient between the glass fiber and the trench. Due to the edge jaggedness of the trench, ~3 μm

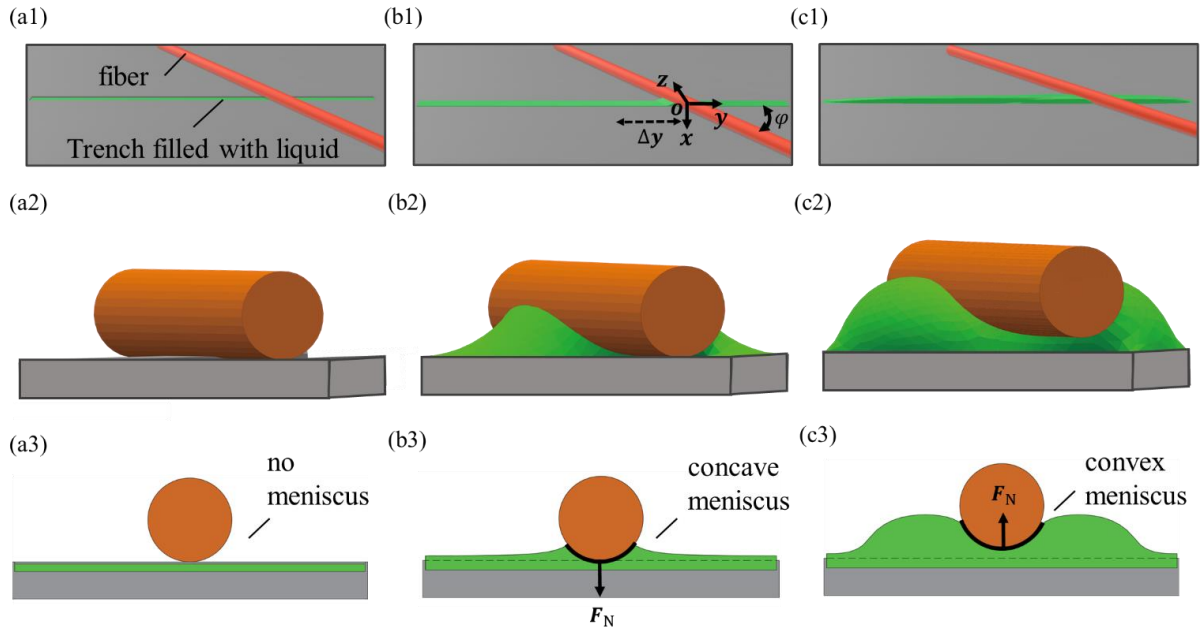

Fig. 3. Analysis and simulation of droplet directed self-alignment of microfiber to super hydrophilic-superhydrophobic micro trench: (a1) - (a3) the fiber has no contact with the liquid surface and no meniscus is formed; (b1) - (b3) the fiber is in contact with the liquid and a concave meniscus is formed; (c1) - (c3) the fiber is in contact with the liquid surface and a convex meniscus is formed.

wide and ~2 μm high, the friction force will act mostly from the edges of trench instead of the substrate. Considering that the friction coefficient of aluminum and steel surface with ridges could reach 1.1 -1.6 [23], the counter-torque caused by the friction forces can be calculated as $T_f = f d_f = \mu F_N w/2sin\varphi$, where d_f is the distance between the point of action to the cross point O, and w is the width of the trench (see Fig. 4(a)). Fig. 4 (b) shows the Surface Evolver simulation of the counter-torque T_f caused by the friction forces and the horizontal torque T_C as the function of rotational placement error φ, where the y-axis on the left represents the counter-torque and the y-axis on the right represents the horizontal torque. In the simulation, the volume of water meniscus was 0.02 nL, and the distance between the fiber and the trench Δz was set to equal the radius of the fiber (7.5 μm) since the fiber is in contact with the trench.

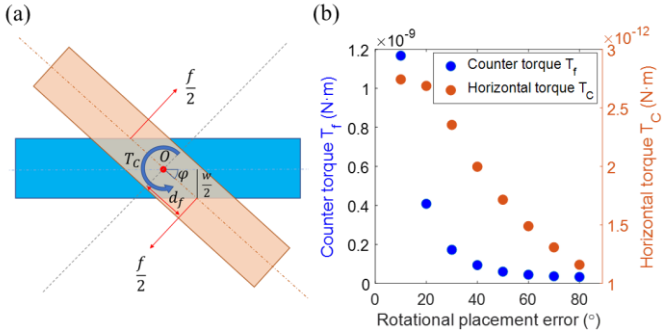

Fig. 4. Illustration of counter-torque caused by friction forces and horizontal torque from meniscus: (a) analysis of friction forces and horizontal torque; (b) the counter-torque and the horizontal torque acting on the fiber as the function of rotational placement error.

The results show that the counter-torque T_f caused by friction forces is about three orders of magnitude greater than the horizontal torque T_C, therefore, leading to no motion of the fiber.

In the third scenario as shown in (Fig. 3 (c1)-(c3)), the water meniscus increases further, and eventually, the shape of the meniscus is convex. During this process, the vertical component of the capillary force F_N will firstly decrease in value and finally change its direction pointing upwards and lift the fiber. In such a scenario, a water film may exist between the fiber and trench. The horizontal torque T_C will drive the fiber to rotate around the crossing point of the fiber and the trench. The rotational direction of the fiber is decided by the angular difference between the fiber and the trench or the rotational placement error φ. When $\varphi < 90°$, the fiber will rotate anticlockwise, on the other hand, when $\varphi > 90°$, the fiber will rotate clockwise.

Fig. 5 shows the simulation of the free surface energy E of the meniscus and the respective horizontal torque T_C acting on the fiber as a function of rotational placement error φ based on Eq. (2). The calculation of torque is a coarse approximation using energy values at 10 degrees spacing. As shown in Fig. 5 (a), the surface energy of the water meniscus decreases as the rotational placement error decreases, and it is minimized as the error decreases to zero. Fig. 5 (b) shows the horizontal torque, which drops to zero when the rotational error becomes zero,

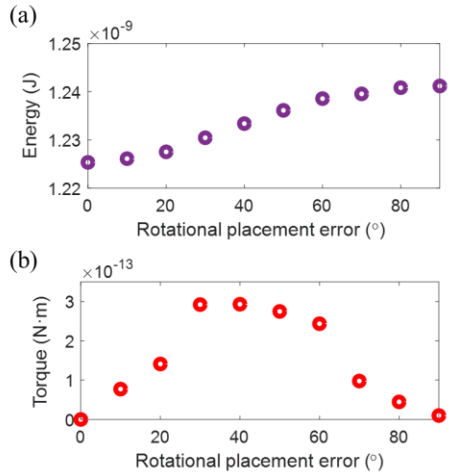

Fig. 5. Surface Evolver simulation of a meniscus between a fiber and a trench in the third scenario: (a) surface energy of the meniscus as the function of rotational placement error; (b) torque acting on the fiber as the function of rotational placement error.

indicating that the horizontal torque will drive the fiber to rotate until it is aligned to the trench. In the simulation, the volume of water meniscus is 5 nL, and the distance between the fiber and the trench Δz is set to the value where the capillary force in the vertical direction $F_Z = -\nabla E(\Delta z)$ is balanced with the gravity of the fiber such that $F_Z = G$, where $G = \rho l_0 \pi (\frac{d}{2})^2 g = 0.013$ μN, l_0 is the length of the fiber, ρ is the mass density of glass ($2500\ kg/m^3$), d is the diameter of the fiber, g is the gravity acceleration.

Since there is only torque in the x-y plane, the fiber will only rotate and there is no displacement during the first phase of the process. After the rotational placement error is mostly corrected and at least an end of fiber contacts the meniscus, the second phase of the process starts. In Fig. 6, we show the change of energy and force when the fiber linearly transports into the trench reducing the linear displacement error Δy. The driving force correcting the displacement error can also be derived from surface energy obtained from Surface Evolver simulation (Fig. 6 (a)) using Eq.(1). Fig. 6 (b) shows the surface energy as the function of the displacement error Δy. As the displacement

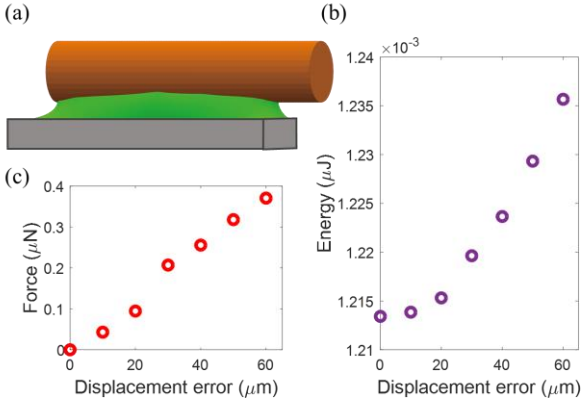

Fig. 6. Simulation of a fiber on a trench with linear displacement error: (a) surface evolver simulation; (b) surface energy as the function of the displacement error; (c) driving force as the function of the displacement error.

error decreases to zero, the surface energy of the meniscus is minimized, and the fiber is transported into the trench. Fig. 6 (c) shows that the driving force for transporting the fiber decreases as the displacement error decreases, and the force drops to zero as the displacement error Δy decreases to zero.

The simulations indicate critical condition for successful self-alignment and transportation of microfiber to the micro trench. The condition is that there should be enough water forming a water film between the fiber and the trench so that the capillary force plays a dominant role. Therefore, it is favorable to add more water to the meniscus to form a convex meniscus between the fiber and the trench. The analysis indicates that the rotational placement error will be corrected at first and then the displacement error will be corrected. The rotational direction of the fiber mainly depends on the initial rotational placement error φ. The surface energy of the water meniscus between the microfiber and the trench is minimized when both the displacement error and rotational placement error become zero. It is worth noting that when $\varphi < 0.5°$, we have $\varphi \cdot l_0/2 \approx w$, where l_0 and w are the length and width of the fiber respectively, the translational error and rotational error could be corrected simultaneously, similar to the cases of chip self-alignment [24]. Since the angle is rather small, so we do not discuss this as a separate phase.

IV. Experimental Results

We experimentally investigated the proposed ejected droplet directed self-alignment and transportation of microfibers using a non-contact dispenser. Fig. 7 shows the general self-alignment procedure of a 3 mm long and 15 μm in diameter glass fiber to a shape matching super hydrophilic-super hydrophobic trench with a width of about 20 μm and a depth of 8 μm. Firstly, a microfiber was placed next to a trench randomly (Fig. 7 (a)); then a series of droplets were dispensed in the trench by the dispenser (Fig. 7 (b)); the water meniscus spread and fully wetted the trench and the fiber was self-aligned and transported into the trench (Fig. 7 (c)); finally, the water droplets evaporated, and the fiber remained inside the trench (Fig. 7 (d)). A zoomed optical image of the aligned fiber inside the trench is shown in Fig. 7 (e). A demonstration of the droplet directed self-alignment of a microfiber to a super hydrophilic trench is shown in the supplementary video (Movie S1). The volume of the droplet ejected into the trench is approximately 5 nL, which was chosen based on the simulation results shown in Fig. 3 (c). This volume can usually start rotating the fiber. Additional volume may be delivered in some cases to ensure the successful completion of the whole process. In addition, Fig. 7 shows that the end of the fiber may be in contact with the substrate. However, such contact can be overcome by delivering additional amount of droplets into the trench. We attribute this to the lifting of the fiber by a sufficiently large meniscus. In experiments, the actual delivered volume varies from 5-8 nL.

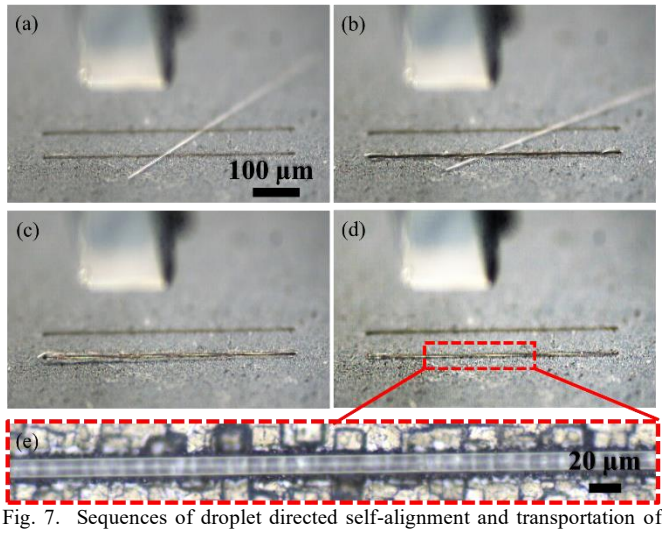

Fig. 7. Sequences of droplet directed self-alignment and transportation of microfiber: (a) a microfiber was placed next to a trench; (b) a series of droplets were dispensed in the trench by a non-contact dispenser, the droplets quickly spread in the trench; (c) the fiber was self-aligned to and transported inside the trench; (d) the water in the trench evaporated and the fiber was inside the trench; (e) a zoomed optical image of the aligned microfiber inside the trench. (Movie S1)

A. Experimental Validation of Mechanism

Series of experiments were carried out to study the mechanism of the droplet directed transportation and self-alignment of microfibers. Fig. 8 shows four scenarios of droplet directed self-alignment and transportation of microfibers to super hydrophilic-super hydrophobic trenches. In the first scenario as shown in Fig. 8 (a), when the trench was fully wetted by the droplets, the fiber was self-aligned and transported into the trench in one round. The theoretical analysis indicates that the rotational placement error will be corrected at first and then the displacement error will be corrected. The reason for the seemingly synchronized rotational movement and the displace movement in the first scenario are most likely due to the fast speed of the rotational and displace movements, so the camera could not catch the sequences of two movements.

In the second scenario (Fig. 8 (b)), the fiber firstly moved towards the trench but with a small rotational placement error and a displacement error left, and the fiber was aligned with and transported to the trench in the second round. This may be caused by the jagged edges of the trench. The microfiber may get stuck during the self-alignment process and require more liquid to lift it until the fiber is higher than the jagged edge.

In the third scenario (Fig. 8 (c)), the rotational placement error was firstly corrected with part of the fiber inside the trench and part of the fiber out of the trench, right after that, the displacement error was corrected, and the fiber was transported into the trench in the second round. The third scenario is consistent with the theoretical analysis, which indicates that the rotational placement error will be corrected at first and then the displacement error will be corrected.

The fourth scenario (Fig. 8 (d)) represents an extreme case of large displacement error and rotational placement error, where only the end of the fiber was in touch with the trench. Nevertheless, the fiber was still able to align and transport into the trench in one round.

To sum up, the experimental results show that the initial position of the microfiber against trench does not hamper the droplet directed self-alignment and transportation process. Both

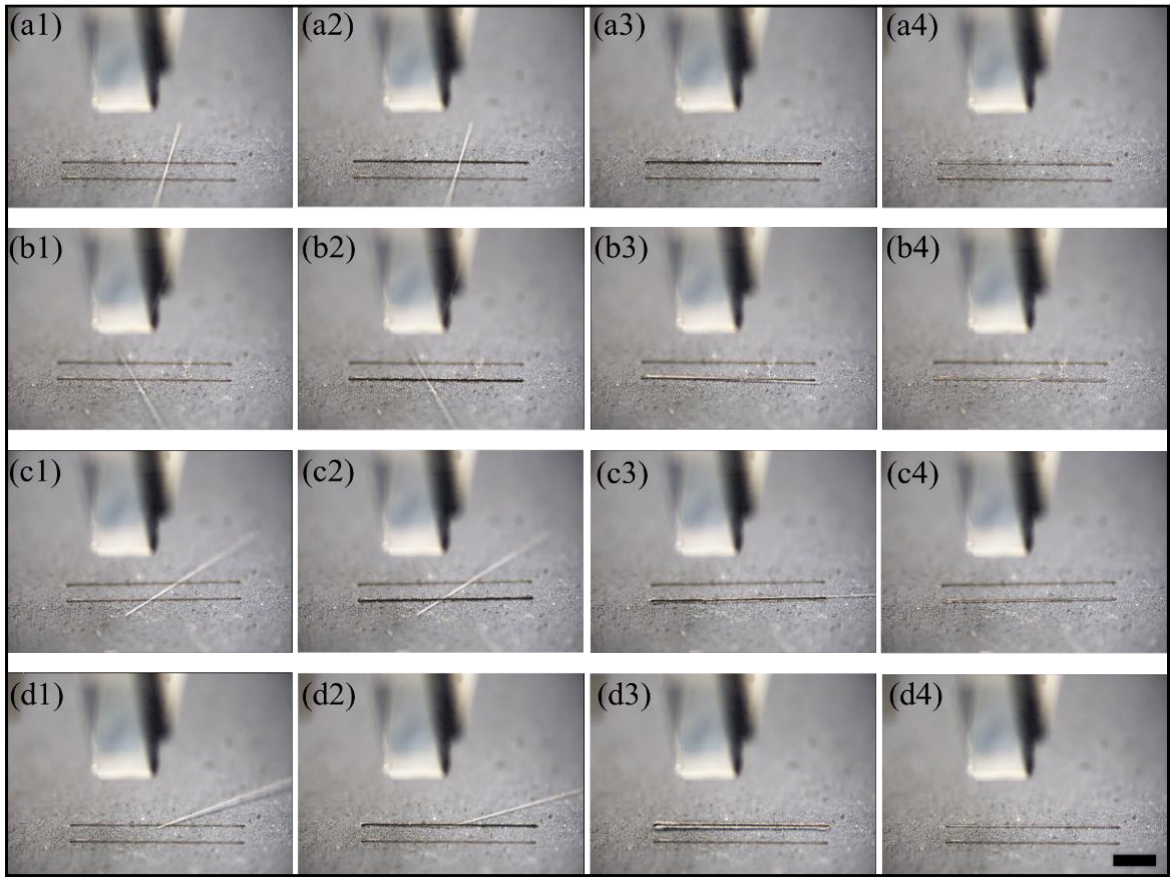

Fig. 8. Four scenarios of droplet directed transportation and self-alignment of microfiber: (a) 1st scenario: both rotational placement error and displacement error were corrected simultaneously; (b) 2nd scenario: self-alignment was achieved in two rounds; (c) 3rd scenario: the rotational placement error was firstly corrected, and the displacement error was corrected afterwards; (d) 4th scenario: self-alignment can be achieved with extreme large displacement and rotational placement error. Scalar bar: 500 μm.

displacement error and rotational placement error can be corrected, where the rotational placement error is normally firstly corrected and then the displacement error is corrected. The self-alignment can also be achieved with extreme large displacement error and rotational placement error. The dynamics in different scenarios are most likely caused by the manufacturing defects around the edges of the micro trenches.

B. Influence of Contact Angle of Trench on Wetting Speed

To achieve the droplet directed self-alignment, another key factor is that the liquid droplets should wet the trench and take the shape of the trench. We carried out tests to study the influence of the contact angle of the trench on the wetting speed of the droplets in the trench. We fabricated the trench with the water contact angle of 10°, 25°, 90°, 130°. The size of the trench used in the experiment is 100 μm in width, 3 mm in length. A non-contact dispenser was used to dispense droplets at the center of the trench. The wetting of the trench with different contact angles are shown in Fig. 9. When the water contact angle of the trench is 10°, the trench was fully wetted by the droplets in less than 80 milliseconds (Fig. 9 (a)). A fast speed video of the droplets fully wetting a super hydrophilic trench is shown in the supplementary video (Movie S2).

As the water contact angle of the trench increases to 25°, only a small portion of the trench was wetted (Fig. 9 (b)). When the trench is hydrophobic, droplets do not spread in the trench at all (Fig. 9 (c)-(d)). When the contact angle of the trench is 10°, it takes about 76±2 milliseconds to fully wet the trench. The results indicate that it is preferable that the trench is super hydrophilic, so that the trench can be evenly fully wetted by the water droplets for the droplet directly self-alignment of microfiber. It is worth noting that the volume of the droplet should not exceed the maximum volume of the droplet that can

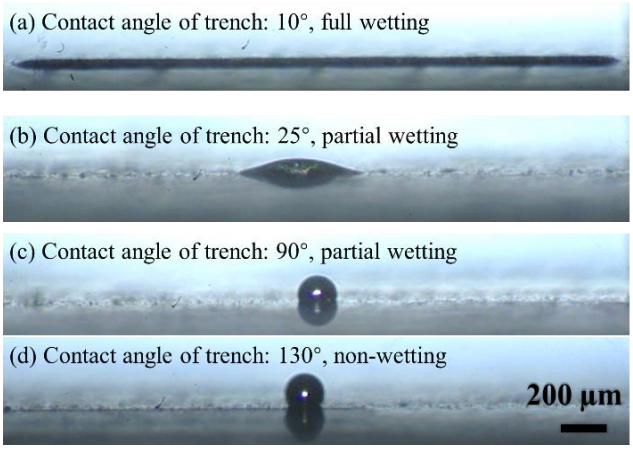

Fig. 9. Wetting of droplets in a 3 mm long trench with water contact angle of (a) 10° (b) 25° (c) 90° (d) 130°. (Supplementary Video: Movie S2)

be confined inside the trench in order to ensure the stability of the meniscus shape [24] and achieve reliable self-alignment.

C. *Influence of Size of Trench on Alignment Accuracy*

We have further investigated the alignment accuracy of the microfiber on the shape matching trench with the width of 20 μm, 40 μm and 60 μm, the depth of 8 μm and the length of 3 mm. The trenches with the water contact angle of 10° were used in the experiments. The alignment accuracy consists of both linear alignment accuracy and angular alignment accuracy. The linear alignment accuracy is defined as the difference between the center of the fiber and the center of the trench along the width of the trench. The angular alignment accuracy is the difference in angle between the fiber and the trench. Fig. 10 shows the aligned fibers to the shape matching trench with different widths, where the yellow dotted lines represent the edges of the trench.

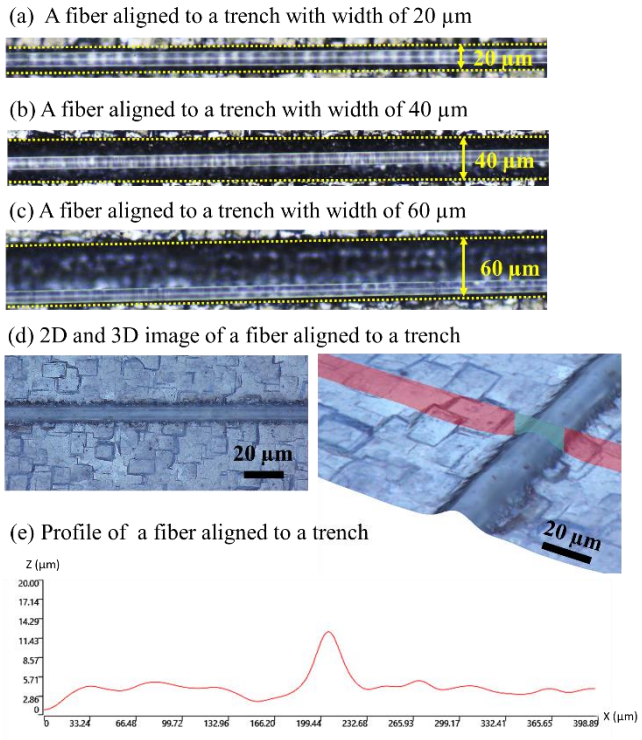

Fig. 10. Alignment accuracy of a microfiber on shape matching super hydrophilic trench with different width: (a) aligned fiber to a 20 μm wide trench; (b) aligned fiber to a 40 μm wide trench; (c) aligned fiber to a 60 μm wide trench; (d) 2D and 3D image of a fiber aligned to a 20 μm wide trench; (e) profile of a fiber aligned to a 20 μm wide trench.

Each test was repeated 5 times. The results are summarized in Table I. The results indicate that both the angular alignment accuracy and linear alignment accuracy are improved as the width of the trench decreases. When the width of the trench is 20 μm, the angular alignment accuracy is about 0.1° and the linear alignment accuracy is about 0.5 μm. It appears that the better the width of the trench matches the diameter of the fiber, the better the alignment accuracy can be achieved. Furthermore, the length of the fiber also could influence alignment accuracy. The better the fiber length matches the trench length, the higher the alignment accuracy along the trench's length can be reached, as well as the rotational accuracy.

TABLE I
ALIGNMENT ACCURACY OF DROPLET DIRECTED SELF-ALIGNMENT OF MICROFIBER

Width of trench (μm)	Linear alignment accuracy (μm)	Angular alignment accuracy (°)
20	0.5±0.1	0.1±0.1
40	5.5±0.4	1.5±0.2
60	21.5±4.5	3.5±0.4

D. *Demonstration of Fiber Alignment*

We conducted tests to demonstrate the proposed capillary self-alignment method. Fig. 11 (a)-(b) show self-alignment of a human hair having a diameter of 90 μm and a length of 4 mm. The human hair was firstly placed on a super hydrophilic-super hydrophobic trench randomly, and then the hair was self-aligned to the trench with a diameter of 100 μm and a length of 4 mm. It is worth noting that the self-alignment procedure can still be accomplished even when the human hair is curved. The end of the hair, however, may bend upwards from the trench to its original curved shape when the water droplet evaporates. Non-volatile liquids or adhesives should be used to keep the aligned hair from bending back to its original shape. Fig. 11 (c) – (e) demonstrate the construction of different patterns using multiple fibers, including four fibers distributed in a zigzag pattern, 10 fibers aligned in parallel and 18 fibers aligned to a "SUST" logo. The alignment of multiple fibers was done as follows: firstly, the fibers were coarsely placed on the substrate manually with one fiber for each trench at random orientation; then water droplets were dispensed to the trenches one by one, making each fiber self-align to its corresponding trench. We believe this method could be applied in a batch process for high throughput self-alignment. All the fibers utilized in the demonstration have a diameter of 15 μm and a length of 2 mm to 4 mm. The presentation demonstrates that the proposed capillary self-alignment method can construct complex patterns with microfibers, which could lead to applications such as fiber-based microsensors, fiber-reinforced materials, and so on.

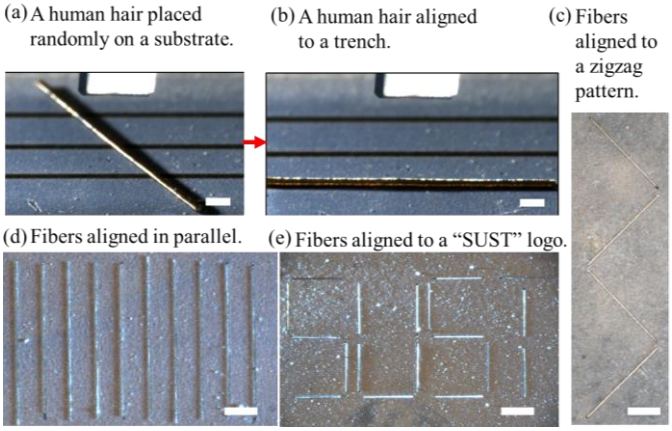

Fig. 11. Demonstration of fiber alignment: (a) a human hair is placed randomly on a substrate; (b) a human hair is aligned to a 100 μm wide trench; (c) four fibers are aligned to a zigzag pattern; (d) ten fibers are aligned in parallel; (e) 18 fibers are aligned to a "SUST" logo. Scalar bar: 200 μm.

V. CONCLUSIONS

In conclusion, this work reported a facile droplet directed method which can align and transport randomly dispersed

fibers around trenches into the trenches as desired. The proposed method requires no actual location of the fiber, neither the actual location of the point of cross of the fiber on the trench, but only the fiber being partially on the trench and the liquid being ejected into the trench. Liquid volume is critical to allow the capillary force to be dominant leading to the success of the self-alignment and transportation process. The proposed droplet-directed self-alignment method can achieve accurate positioning and fast alignment of microfibers, which leads to great potential for larger scale and high-throughput construction of complex microstructures using microfibers.

Even though the medium used in this study is water, other liquid such as oil or adhesives should also work as shown in the previous studies of self-alignment of microchips [18]. Many hydrophobic surfaces are oleophilic, so if we use oil-based solution or adhesive as the medium, the proposed method can be extended for hydrophobic fibers. Of course, the trench should confine the solution or adhesive. We believe the topological structure used in the paper should confine oil or adhesive to certain extent, as reported in previous publications [18]. The proposed method should also be applicable to soft fibers if the fiber is not heavily curved. For the curved microfibers, non-volatile liquids or adhesive could be employed for capillary self-alignment.

REFERENCES

[1] J. Greenhall, F. Guevara Vasquez, and B. Raeymaekers, "Ultrasound directed self-assembly of user-specified patterns of nanoparticles dispersed in a fluid medium," *Appl. Phys. Lett.*, 2016.

[2] P. Gupta, M. Rajput, N. Singla, V. Kumar, and D. Lahiri, "Electric field and current assisted alignment of CNT inside polymer matrix and its effects on electrical and mechanical properties," *Polymer (Guildf).*, vol. 89, pp. 119–127, 2016.

[3] J. E. Fischer *et al.*, "Magnetically aligned single wall carbon nanotube films: Preferred orientation and anisotropic transport properties," *J. Appl. Phys.*, vol. 93, no. 4, pp. 2157–2163, 2003.

[4] Y. Liu, X. Zhang, Y. Xia, and H. Yang, "Magnetic-field-assisted electrospinning of aligned straight and wavy polymeric nanofibers," *Adv. Mater.*, 2010.

[5] C. Pang *et al.*, "A flexible and highly sensitive strain-gauge sensor using reversible interlocking of nanofibres," *Nat. Mater.*, vol. 11, no. 9, pp. 795–801, 2012.

[6] L. Sainiemi *et al.*, "Non-reflecting silicon and polymer surfaces by plasma etching and replication," *Adv. Mater.*, vol. 23, pp. 122–126, 2011.

[7] Y. Yu *et al.*, "Fabrication and characterization of electrospinning/3D printing bone tissue engineering scaffold," *RSC Adv.*, vol. 6, no. 112, pp. 110557–110565, 2016.

[8] J. Hirvonen, M. Von Essen, and P. Kallio, "Automated microrobotic manipulation of paper fiber bonds," in *IEEE International Conference on Intelligent Robots and Systems*, 2015.

[9] T. Sun, X. Li, Q. Shi, H. Wang, Q. Huang, and T. Fukuda, "Microfluidic Spun Alginate Hydrogel Microfibers and Their Application in Tissue Engineering," *Gels*, vol. 4, no. 2, p. 38, 2018.

[10] R. J. Knuesel and H. O. Jacobs, "Self-assembly of microscopic chiplets at a liquid-liquid-solid interface forming a flexible segmented monocrystalline solar cell.," *Proc. Natl. Acad. Sci. U. S. A.*, vol. 107, pp. 993–998, 2010.

[11] S. C. Park, J. Fang, S. Biswas, M. Mozafari, T. Stauden, and H. O. Jacobs, "A first implementation of an automated reel-to-reel fluidic self-assembly machine," *Adv. Mater.*, pp. 5942–5949, 2014.

[12] Q. Zhou, "Hybrid microassembly for 3D integration and heterogeneous integration of microsystem – EU FP7 Project FAB2ASM," *Proc. Smart Syst. Integr.*, 2013.

[13] D. H. Gracias, V. Kavthekar, J. C. Love, K. E. Paul, and G. M. Whitesides, "Fabrication of Micrometer-Scale, Patterned Polyhedra by Self-Assembly," *Adv. Mater.*, vol. 14, no. 3, pp. 235–238, Feb. 2002.

[14] C. J. Morris, S. a. Stauth, and B. a. Parviz, "Self-assembly for microscale and nanoscale packaging: steps toward self-packaging," *IEEE Trans. Adv. Packag.*, vol. 28, no. 4, pp. 600–611, Nov. 2005.

[15] Y. Ito, T. Fukushima, K. W. Lee, T. Tanaka, and M. Koyanagi, "Capillary Self-Assembly for 3D Heterogeneous System Integration and Packaging," in *MRS Advances*, 2016.

[16] H. J. J. Yeh and J. S. Smith, "Fluidic self-assembly for the integration of GaAs light-emitting diodes on Si substrates," *IEEE Photonics Technol. Lett.*, vol. 6, no. 6, pp. 706–708, 1994.

[17] R. R. Chaudhuri, Y. Song, and S. W. Seo, "Heterogeneously integrated optical detection platform for on-chip sensing applications," *J. Opt. (United Kingdom)*, 2015.

[18] M. Mastrangeli, Q. Zhou, V. Sariola, and P. Lambert, "Surface tension-driven self-alignment," *Soft Matter*, vol. 13, no. 2, pp. 304–327, 2017.

[19] B. Chang, B. K. Wang, J. L. Jin, and Q. Zhou, "Capillary Pick-and-Place of Glass Microfibers," *IEEE Access*, vol. 9, pp. 15074–15083, 2021.

[20] B. Chang, J. Jin, and Q. Zhou, "Surface tension-based alignment of microfibers on hydrophilic–superhydrophobic grooved surfaces," *Micromachines*, vol. 11, no. 11, pp. 1–12, 2020.

[21] A. Y. Vorobyev and C. Guo, "Laser Makes Silicon Superwicking," *Opt. Photonics News*, vol. 21, no. 12, p. 38, 2010.

[22] K. A. Brakke, "The Surface Evolver," *Exp. Math.*, vol. 1, pp. 141–165, 1992.

[23] U. Pettersson, *Surfaces Designed for High and Low Friction*. 2005.

[24] G. Arutinov, E. C. P. Smits, P. Albert, P. Lambert, and M. Mastrangeli, "In-plane mode dynamics of capillary self-alignment," *Langmuir*, vol. 30, no. 43, pp. 13092–13102, 2014.

Bo Chang received the M.S. degree in automation technology from Tampere University of Technology, Finland, and the Dr. Tech. degree in electrical engineering from Aalto University, Finland.

From 2013 to 2016, she was an Academy Postdoctoral Researcher with the Robotic Instruments Laboratory, Aalto University, Finland. Since 2017, she has been a Professor with the School of Mechatronics Engineering, Shaanxi University of Science and Technology. Her research interests include robotic microassembly, self-assembly, micromanipulation, micro-robotics and applications.

Yu H. Feng received the B.S. degree in mechanical design manufacturing and automation technology from Shaanxi University of Science and Technology, Xi'an, China in 2019. He is currently a master student in the School of Mechatronics Engineering, Shaanxi University of Science and Technology, Xi'an, China.

His research interests include laser microfabrication and microassembly.

Jia L. Jin received the B.S. degree in mechanical design manufacturing and automation technology from Shaanxi University of Science and Technology, Xi'an, China in 2018. He is currently a master student in the School of Mechatronics Engineering, Shaanxi University of Science and Technology, Xi'an, China.

His research interests include micromanipulation and microassembly.

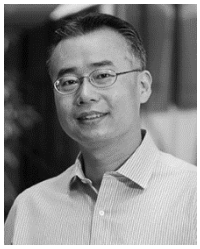

Quan Zhou received the M.S. degree in control engineering and the Dr. Tech. degree in automation technology, both from Tampere University of Technology, Tampere, Finland. Currently, he is an associate professor leading the Robotic Instrument Group at the Department of Electrical Engineering and Automation, School of Electrical Engineering, Aalto University, Finland. His main research interests include miniaturized robotic instruments, micromanipulation and related automation methods.

He is currently the coordinator of the Miniaturized Robotics Topic Group of European Robotics Association (euRobotics). He was also the General Chair of International Conference on Manipulation, Automation and Robotics at Small Scales, MARSS 2019. Prof. Zhou was also the coordinator of EU FP7 project FAB2ASM, the first PPP project of the European Economic Recovery Plan. He was also the Chair of IEEE Finland Joint Chapter of Control System Society, Robotics and Automation Society and System Man and Cybernetics Society.